J Musculoskelet Neuronal Interact 2025; 25(4):371-376

Journal of Musculoskeletal and Neuronal Interactions JMNI

Original Article

Assessment of Local Pelvic Bone Volumetric Density and Cortical Thickness Using Multi-Energy Bi-Planar Radiography

Ningxin Qiao[1,2], Isabelle Villemure[1,2], Carolina Solorzano Barrera[3], Carl-Eric Aubin[1,2,3]

[1]Institute of Biomedical Engineering, Polytechnique Montreal, Montreal, Canada;
[2]Sainte-Justine University Hospital, Research Center, Montreal, Canada;
[3]Department of Mechanical Engineering, Polytechnique Montreal, Montreal, Canada

Abstract

Objective: This study presents a method to determine the volumetric density of pelvic bone and cortical bone thickness along critical regions of the S2 alar-iliac (S2AI) screw trajectory using bi-planar multi-energy X-ray (BMEX). **Methods**: Simulated BMEXs were generated from CT data from eight patients, with coordinate matching linking pixels to voxel density values. This dataset included pixel attenuation values, coordinates as independent variables, and voxel attenuation values (Hounsfield Units, HU) as the dependent variable for training a random forest regressor model. **Results**: The trained model revealed adequate trabecular bone density prediction (root mean square error: 32.8 mg/cm^3) and cortical thickness accuracy (error ≤ 1.2 mm). Trabecular bone showed a minor tendency for density overestimation with a maximum difference of 83 HU, while cortical bone exhibited an underestimation of up to 118 HU. **Conclusions**: The improved prediction of bone density and the capability to estimate cortical bone thickness signify a significant advancement towards a comprehensive modality for predicting bone quality in implant placement planning.

Keywords: Adult Spine Deformity, Bi-planar Multi-energy X-ray, Random Forest Regressor, Volumetric Bone Density

Introduction

A significant proportion of the population with previously normal spinal curvature is affected pathologically with age[1], and this proportion increases with the aging of the population. In severe cases, adult spinal deformities (ASD) require surgery, which involves inserting pedicle screws into the vertebrae connected to rods to correct spinal deformities and maintain postoperative balance and stability. In cases of significant imbalance long instrumentation extending to the pelvis is necessary, with sacral and/or S2-alar-iliac (S2AI) screws. Surgical planning in the treatment of ASD is important because of the occurrence of post-surgery complications[2,3]. Among the major complications that are frequently encountered, pelvic screw loosening is particularly noteworthy, as it is closely associated with osteoporosis[2-5].

The planar nature of X-ray imaging limits its ability to interpret 3D bone density associated with spino-pelvic pathology. This also limits its potential use for biomechanical analysis, such as finite element analysis (FEA). Bi-planar multi-energy X-ray (BMEX) is a recent technique that provides separate planar images of bone and soft tissues in posterior-anterior and lateral views for the comprehensive evaluation of spinal and pelvic pathology[6], providing information on bone deformities, spinal-pelvic alignment and curvature, as well as information on bone density. While calibrated CT-scans remain a valid and well-established approach for assessing bone density, BMEX is

Dr. Aubin reports grants from the Natural Sciences and Engineering Research Counsil of Canada (Alliance University-Industry Grant with Medtronic of Canada), and outside of the current work, contracts with Medtronic. Dr. Villemure, Mr. Qiao and Ms. Solorzano Barrera have nothing to declare.

Corresponding author: Carl-Eric Aubin, PhD., P.Eng., Full Professor, Polytechnique Montréal, PO Box 6079, Downtown station, Montréal, QC H3C 3A7, Canada
E-mail: carl-eric.aubin@polymtl.ca

Edited by: G. Lyritis
Accepted 13 July 2025

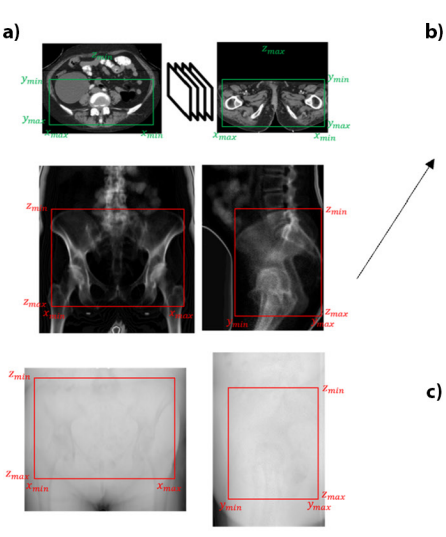

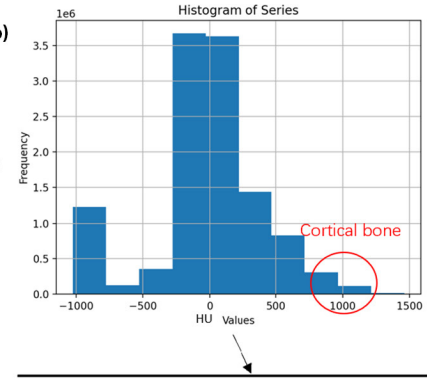

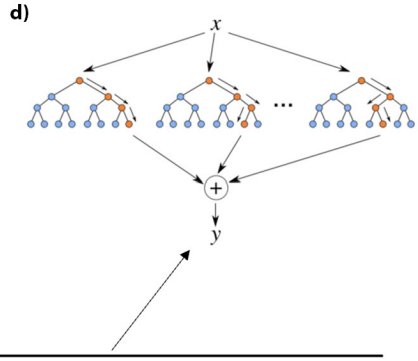

c)

PA Bone pixel intensity	LAT Bone pixel intensity	PA Soft Tissue pixel intensity	LAT Soft Tissue pixel intensity	x*	y*	z*	Volumetric density (HU)
8159	18107	47027	44592	0.18	0.78	0.27	-21
28900	8666	39983	43570	0.91	0.02	0.23	2
1299	1287	48642	50158	0.34	0.03	0.47	-49
2198	11742	48473	54554	0.34	0.23	0.48	-68
13389	12542	45939	47388	0.50	0.73	0.74	24

*normalized coordinates rounded to 2 decimal places.

Figure 1. Calibration process between CT-scans and BMEXs; a) Match the CT scans (top row, in green) with the BMEX images (middle and bottom rows, in red); b) Conduct a histogram analysis of CT-scans; c) Create the dataset. The table presents examples for 5 distinct voxels (volumetric density in HU) and their respective values of independent variables; d) Apply the machine learning model (random forest).

of particular interest to clinicians and orthopaedists as it provides rapid acquisitions with low-dose radiation as well as bone density estimation, which are key to image large bone areas of interest such as the instrumented spine. BMEX was used in a few studies to estimate trabecular volumetric bone mineral density (vBMD) for FEA[6-8], and personalized FEA was subsequently used to optimize the S2AI trajectory and minimize the potential for loosening[9]. Limitations of these studies include a high root mean square error (RMSE) in vBMD estimation and a lack of provided information on cortical bone thickness. The objective of this study was to accurately predict trabecular and cortical bone density and cortical bone thickness from BMEX, with a view to incorporating this data into a patient-specific finite element model for biomechanical studies of ASD.

Materials and Methods

To control all study parameters and possible acquisition uncertainties found during practice, simulated analytical BMEXs were generated using a vendor-specific image simulator. This simulator consists of a dedicated software tool that uses patient CT-scans as input, along with configurable imaging acquisition parameters specific to the BMEX system. Synthetic images were generated by mapping voxel values to pixel intensities in a planar projection. Finally, the resulting BMEX images were automatically calibrated with hydroxyapatite density to synthetically simulate bone mineral density[8].

This project utilizes CT-scan data from four male and four female cases with a mean BMD of 0.17 ± 0.02 g/cm^3 from the Cancer Imaging Archive[10], which provides publicly available de-identified images for research; it was therefore not necessary to obtain institutional and ethics board approval for this project. The selected cases served to illustrate the feasibility of the proposed workflow in a proof-of-concept setting. Additional patient characteristics were not available in the archive. However, the model was designed to rely solely on imaging data, with voxel characteristics sufficient to define intensity thresholds and anatomical features for prediction. Manual definition of pelvic extent was performed on both CT scans and the corresponding simulated BMEXs (postero-anterior and lateral views). Subsequently, the coordinates from the simulated BMEXs were adjusted to align with those of the CT scans. Histogram analysis was conducted to determine the appropriate adjustments for downsizing and upsizing, ensuring that the feature of interest, particularly cortical bone, was not overwhelmed by features of non-interest, such as voxels of soft tissues. Multiple iterations were performed to empirically determine the optimal up-sampling and down-sampling factors required to balance voxel classes and refine model predictions. As there were very few voxels corresponding to the cortical bone, which is the feature of interest for extraction, they were up-sampled by a factor of 2. On the other hand, there was

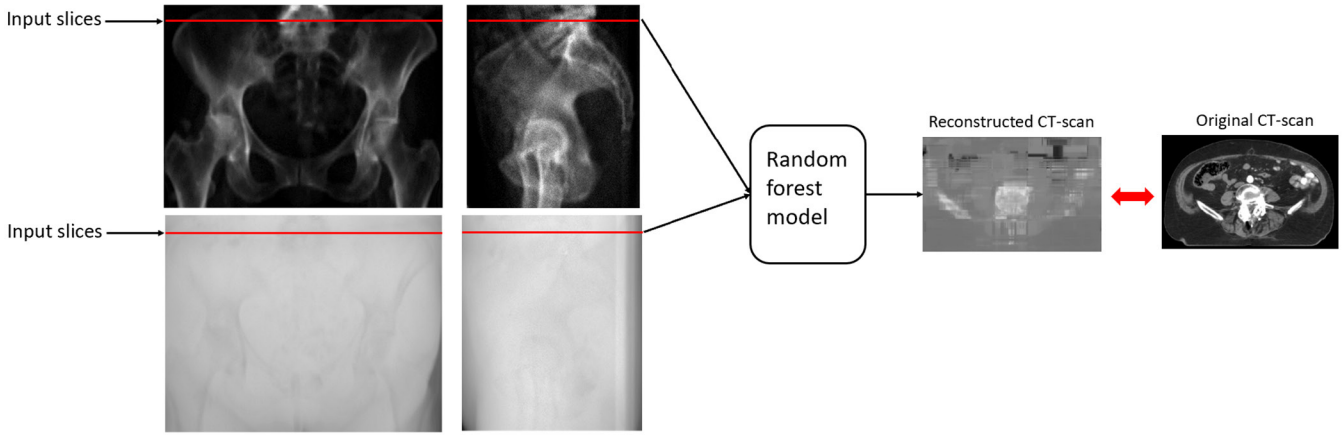

Figure 2. Example of the simulation of a reconstructed CT-scan slice from BMEX (left/top) and corresponding CT images (right/bottom), compared with the corresponding original CT-scan slice.

a large number of voxels around 0 Hounsfield Unit (HU), representing soft tissues less relevant in the context of this study; therefore, they were down-sampled by a factor of 5 (Figure 1).

Using BMEX in posteroanterior (PA) and lateral (LAT) views with distinct bone and soft tissue density intensities, coordinate matching linked each HU value to four pixel intensities derived from the corresponding BMEX images: PA bone density (PA-BMD), LAT bone density (LAT-BMD), PA soft tissue density (PA-ST), and LAT soft tissue density (LAT-ST). Each HU value was additionally assigned a normalized x, y, z position, resulting in seven associated variables (4-pixel intensities and 3 coordinates) for each dependent HU value (Figure 1). The set of voxels associated with their corresponding dependent variables forms the dataset.

The resulting dataset was processed by a random forest regressor for HU value prediction. The random forest regressor is a machine learning model (MLM) that combines the predictions of multiple decision trees[11]. In each tree, the data were recursively partitioned at each node based on the selected features (Figure 1). The final prediction was obtained by averaging the predictions of all the trees for improved accuracy. In this study, 20 decision trees were used to balance computational resources and performance within the context of the in-house facilities available in our lab. A random state of 10 was defined to ensure the model's reproducibility and a default minimal sampling split of 2 for internal nodes was defined as well. Tree depth was reached until all leaves were pure. 60% of the data was used for training, with the remainder for validation. Model performance was assessed using RMSE and mean absolute error (MAE). Feature importance was determined by calculating the total decrease in node impurity across all trees. This impurity decrease represents the reduction in the variability of the dependent variable, typically measured by the mean squared error, as a result of the split. This decrease is weighted by the probability of reaching each node, which is approximated by the proportion of samples that reach that node. Finally, the importance of each feature was expressed as a percentage representing its relative contribution.

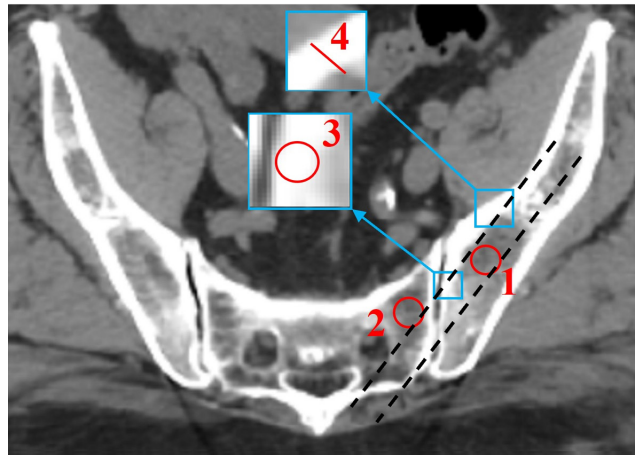

Figure 3. Critical anatomical sites used to evaluate bone density prediction for the use case of the S2-alar-iliac screw trajectory: 1. Body of ilium 2. S2 central ala 3. Cortical ilium at S2 4. Great sciatic notch thickness. The dashed lines enclose a S2-alar-iliac (S2AI) screw trajectory.

Once the model was properly trained, BMEXs (unique data) from four different patients (two males and two females) were used to generate the 3D reconstructed

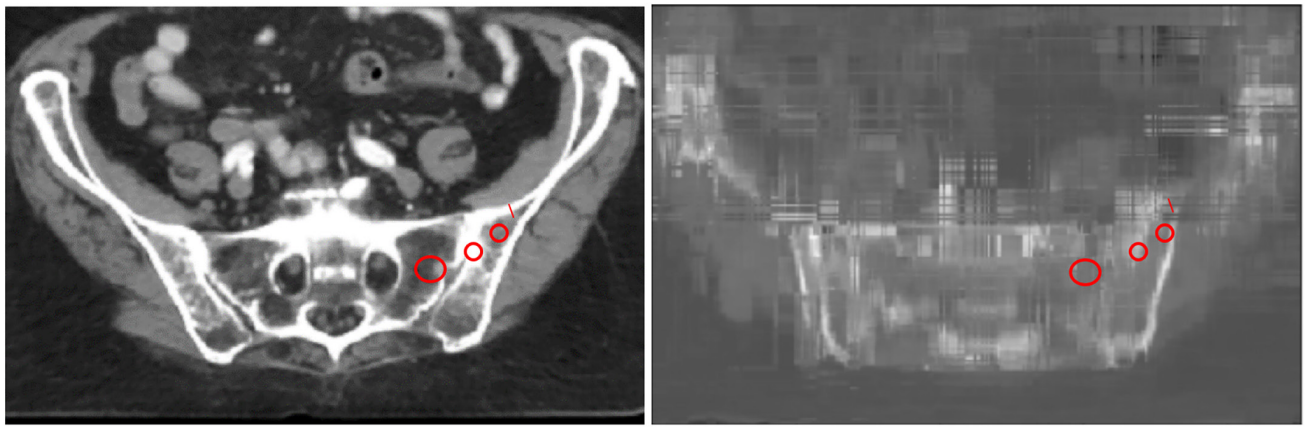

Figure 4. Example of original (left) and reconstructed (right) CT-scan. The area enclosed by red circles and the red line represent the areas and cortical bone thickness of interest for comparison.

Table 1. Difference between the predicted and actual CT scans of average HU values and cortical bone thickness at critical anatomical sites. Positive values indicate higher predicted values than actual values.

Case	Patient gender	Body of ilium (HU)			S2 central ala (HU)			Cortical ilium at S2 (HU)			Great sciatic notch thickness (mm)		
		Actual	Predicted	Difference	Actual	Predicted	Difference	Actual	Predicted	Difference	Actual	Predicted	Difference
1	F	60	88	28	-40	37	77	265	178	-87	5.59	4.78	-0.81
2	F	112	137	25	39	14	-25	349	318	-31	5.35	4.32	-1.03
3	M	228	261	33	0	29	20	322	303	-19	5.41	5.01	-0.4
4	M	124	207	83	-16	53	69	548	430	-118	4.52	3.31	-1.21

volume of the pelvis and compute the associated volumetric density of each voxel and cortical bone thickness, which were subsequently compared with that of the original CT-scans for validation purposes (Figure 2). Pixel spacing (1mm) and slice thickness (3mm) were set identical to the spacing on original CT-scans to ensure consistency. Finally, a verification of the practical utility was carried out for a possible context of surgical use of this new approach by visually comparing the average HU values of critical anatomical sites that lie on a typical S2-alar-iliac screw trajectory. To evaluate trabecular bone density prediction, the HU values from both simulated and original CT scans of these cases were averaged and compared for three anatomical locations of the same size and location (Figure 3). Cortical thickness prediction was manually annotated on the same imaging sets by measuring the perpendicular distance between cortical boundaries defined by abrupt changes in intensity.

Results

The MLM was trained using a dataset consisting of a total of 90,964,542 voxels and their corresponding independent variables. The MLM showed a good match between predictions and actual data, with a tested R^2 of 0.986, a RMSE of 41.5 HU, and a MAE of 20.9 HU.

From the feature importance calculation, the five most important variables were ranked in the following order: LAT-BMD (22.2%), x (17.8%), y (16%), LAT-ST (12.2%), z (11.8%). Additionally, PA-BMD (10.4%) and PA-ST (9.6%) were also identified as significant factors.

An example of verification is shown in Figure 4, where the areas indicated by the red circles for averaging HU values are the same as those selected in Figure 3. These average values were used to compare the original and simulated CT scans, and the red line in the image represents the length considered for the comparison.

The verification of the practical utility at 4 critical

anatomical sites is summarized in Table 1, showcasing the difference between the predicted and actual mean HU values for the ilium body, the S2 central ala, the ilium cortex at S2, and the thickness of the great sciatic notch. Positive values indicate that the predicted values surpass the actual bone values. The results indicate a slight overestimation of up to 83 HU for trabecular bone and an underestimation of up to 118 HU for cortical bone. For the great sciatic notch thickness, the model exhibited a slight underestimation with differences ranging from -1.21 to -0.4 mm.

Discussion

The novel model developed enables to determine pelvic bone volumetric density and cortical bone thickness using multi-energy bi-planar X-rays. This study statistically demonstrated excellent performance, which proves superior to that reported in published studies[6,7] with significantly improved R^2 and RMSE values. Indeed, based on Ruess, Tal's[12] calibration equation $\rho=0.79HU\times10^{-3}$, RMSE and MAE values could be estimated at 32.8 mg/cm^3 and 16.5 mg/cm^3 respectively. In comparison, Choisne, Travert[6] obtained an RMSE of 76 mg/cm^3 in volumetric BMD distribution, using an iterative approach to adjust 18 BMEX-based finite element models (FEMs), and comparing the BMD distribution of BMEX-based FEMs with quantitative computed tomography (qCT)-based FEMs. Also, Qiao, Villemure[7] obtained an R^2 value of 0.418 and an RMSE of 74.7 mg/cm^3 for the regression equation established by a direct correlation between BMEX pixel intensities and CT-scan HU values, sampled from 2,101,584 voxels from CT-scans of 10 patients. Therefore, the enhanced prediction of bone density and the ability to estimate cortical bone thickness represents an important advance towards a comprehensive 3D bone quality prediction modality.

Voxels from 4 male and 4 female patient cases with pelvic morphological differences were utilized to avoid patient-specific biases and to enhance the robustness and applicability of the proposed model. The feature importance analysis revealed that the pixel intensities on LAT-BMD play a crucial role in predicting the corresponding voxel values. This finding aligns with the results of Choisne, Travert[6], who also observed a higher correlation using lateral images compared to PA images. Notably, this study is the first to incorporate spatial coordinates. The analysis of feature importance highlighted a significant spatial dependence in the prediction, suggesting that anatomical sites are critical factors influencing the outcomes. To further improve predictions, future studies could increase the number of cases and consider sampling voxels by anatomical regions, enabling a more precise and targeted prediction approach. This approach would allow for a deeper understanding of the specific anatomical factors influencing the results and potentially enhance the accuracy of the model.

From a visual standpoint, the simulated CT scan faithfully replicates the morphology and density of the pelvic region of interest (Figure 4). Despite the presence of certain limitations in resolution, this study enables targeted and accurate prediction of HU values and cortical bone thickness along the S2AI trajectory from PA and LAT BMEX. As shown in Table 1, clinically accepted differences were observed between the predicted and actual HU values at critical anatomical sites for pelvic screw trajectory. Generally, the discrepancy between the prediction and actual values was below 100 HU, corresponding to an estimated difference of approximately 79 mg/cm^3. Variations up to 280 trabecular HU have been observed within practical inter-scanner estimations[13], meaning our values are within acceptable range when considering the variation of CT-scans used for this study's cases, as well as the generated BMEX images. The identification of the cortical region and its thickness was facilitated by analysing drastic changes in HU values, which proved to be relevant for thickness determination. The model was accurate to within 1.2 mm, with slight deviations in predictions from reference data, but consistent with what is observed in overall pelvic cortical thickness measure, thus highlighting clinical meaningful values[14]. Low HU values, such as those found in the body of the ilium and central ala, tended to be slightly overestimated. Conversely, high HU values, such as in the cortical ilium at S2 and the thickness of the great sciatic notch, were slightly underestimated, indicating that model predictions tended to have a narrower range than the actual range. This discrepancy in the data could be explained by different factors, one being the limitation of using simulated BMEX images. Simulated images are CT-scan dependent and thus the pixel resolution could inherently affect the definition of certain anatomical features and thus report a slight discrepancy in the model predictions.

The present study is subject to certain limitations that must be acknowledged. While feasibility was demonstrated across eight morphometrically distinct cases, these do not reflect the full heterogeneity of the ASD population. Future studies integrating patient-specific factors—such as age, musculoskeletal condition, and imaging parameters—could further enhance prediction accuracy. As the prediction model was based solely on imaging data, certain patient characteristics may have had a minor influence on prediction accuracy. A more comprehensive dataset including musculoskeletal health information could further refine trabecular and cortical HU predictions. While the number of cases was sufficient to establish proof-of-concept and demonstrate the feasibility of the approach, future studies using larger cohorts could help strengthen the training process and enhance model validation. Secondly, the use of traditional MLM such as the random forest regressor is limited to handle large datasets, which restricts the number of images included in the analysis to 32 at present. Other characteristics specific to random forests, such as computational costs or data interpretability, might limit their scalability in complex medical imaging contexts. Further work could explore more advanced models, such as mixed-effect random forests (MERF), to address these aspects.

Lastly, the synthetic radiographs obtained by the BMEX simulator could present a limitation when representing real bone density values and corresponding HU predictions. For this study, the simulated data was served to demonstrate feasibility and validate the methodology for bone density estimation. Future *in vivo* acquisitions could enhance image resolution, enable 3D volume reconstruction and improve the prediction of trabecular HU values.

Conclusion

This study presented a random forest regressor model as a proof-of-concept to predict pelvic volumetric bone density and cortical bone thickness from BMEX images, based on key imaging features. These findings open new avenues for improved pelvic screw fixation strategies and the development of patient-specific finite element models for biomechanical analysis in ASD. While promising, this approach requires further clinical validation using larger, more diverse datasets, including *in vivo* BMEX acquisitions, and the establishment of robust imaging protocols for real-world application.

Authors' Contributions

N.Q. Design and realization of the study, analysis of the results and manuscript writing. C.S.B. aided in the manuscript development and editing. I.V. and C.E.A. Conceptualization, Methodology, Analysis, Writing - review & editing, Supervision, Funding acquisition, Project administration. All authors have read and approved the final manuscript.

Funding

The authors disclose peer-reviewed financial support for academic R&D from the Natural Sciences and Engineering Research Council of Canada (NSERC) (industrial research chair program with Medtronic of Canada, and the NSERC-CREATE program).

Acknowledgments

The authors would like to thank Christian Bellefleur, Sophie Labat and Sajjad Rastegar-Talzali for their technical support during this study.

References

1. Cerpa M, Lenke LG, Fehlings MG, Shaffrey CI, Cheung KMC, Carreon LY. Evolution and Advancement of Adult Spinal Deformity Research and Clinical Care: An Overview of the Scoli-RISK-1 Study. Global Spine J. 2019;9(1 Suppl):8S-14S.
2. Patel SA, McDonald CL, Reid DBC, DiSilvestro KJ, Daniels AH, Rihn JA. Complications of Thoracolumbar Adult Spinal Deformity Surgery. JBJS Rev. 2020;8(5):e0214.
3. Zanirato A, Damilano M, Formica M, Piazzolla A, Lovi A, Villafane JH, et al. Complications in adult spine deformity surgery: a systematic review of the recent literature with reporting of aggregated incidences. Eur Spine J. 2018;27(9):2272-84.
4. Tateen A, Bogert J, Koller H, Hempfing A. [Complications of the lumbosacral junction in adult deformity surgery : Indications and technique for posterior and anterior revision surgery]. Orthopade. 2018;47(4):320-9. Epub 2018/03/07. Komplikationen des lumbosakralen Ubergangs bei Korrektur von Erwachsenendeformitaten : Indikation und Technik dorsaler und ventraler Revisionsoperationen.
5. Iijima Y, Kotani T, Sakuma T, Nakayama K, Akazawa T, Kishida S, et al. Risk Factors for Loosening of S2 Alar Iliac Screw: Surgical Outcomes of Adult Spinal Deformity. Asian Spine J. 2020;14(6):864-71.
6. Choisne J, Travert C, Valiadis J-M, Follet Hln, Skalli W. A New Method to Determine Volumetric Bone Mineral Density from Bi-Planar Dual Energy Radiographs Using a Finite Element Model: An Ex-Vivo Study. Journal of Musculoskeletal Research. 2017;20(03):1750003.
7. Qiao N, Villemure I, Aubin CE. A novel method for assigning bone material properties to a comprehensive patient-specific pelvic finite element model using biplanar multi-energy radiographs. Comput Methods Biomech Biomed Engin. 2023:1-12.
8. Solorzano Barrera C, Villemure I, Aubin CE. A Novel Methodology to Estimate Bone Mechanical Properties Using Dual-Energy Imaging to Improve Pedicle Screw Fixation. J Musculoskelet Neuronal Interact. 2023;23(3):316-27.
9. Qiao N, Villemure I, Wang Z, Petit Y, Aubin C-E. Optimization of S2-alar-iliac screw (S2AI) fixation in adult spine deformity using a comprehensive genetic algorithm and finite element model personalized to patient geometry and bone mechanical properties. Spine Deformity. 2024;12(3):595-602.
10. Yorke AA, McDonald GC, Solis D, Guerrero T. Pelvic Reference Data (Version 1). The Cancer Imaging Archive; 2019.
11. Breiman L. Random Forests. Machine Learning. 2001;45:5-32.
12. Ruess M, Tal D, Trabelsi N, Yosibash Z, Rank E. The finite cell method for bone simulations: verification and validation. Biomech Model Mechanobiol. 2012;11(3-4):425-37.
13. Eggermont F, Derikx LC, Free J, van Leeuwen R, van der Linden YM, Verdonschot N, et al. Effect of different CT scanners and settings on femoral failure loads calculated by finite element models. Journal of Orthopaedic Research. 2018;36(8):2288-95.
14. Richards AM, Coleman NW, Knight TA, Belkoff SM, Mears SC. Bone density and cortical thickness in normal, osteopenic, and osteoporotic sacra. J Osteoporos. 2010;2010.